A Parallel Processing Algorithm for Gravity Inversion

N. Frasheri (1), S. Bushati (2), A. Frasheri (3)
(1) Faculty of Information Technology, Polytechnic University of Tirana (nfrasheri@fti.edu.al),
(2) Academy of Sciences of Albania (sbushati@yahoo.com)
(3) Faculty of Geology and Mining, Polytechnic University of Tirana (alfred.frasheri@yahoo.com),

Abstract: *The paper presents results of using MPI parallel processing for the 3D inversion of gravity anomalies seen from a geophysical point of view. The work is done under the FP7 project HP-SEE (http://www.hp-see.eu/). The inversion of geophysical anomalies remains a challenge, and the use of parallel processing can be a tool to achieve better results, "compensating" the complexity of the ill-posed problem of inversion with the increase of volume of calculations. We used a simple iterative algorithm, in each step incrementing the mass density of a single cuboid element of the 3D geosection that gives the best approximation of residual anomaly. Analyzed results from simple synthetic models as well as from complicated field data showed that inverted bodies have sharp contrast with the surrounding medium, while for multi-body anomalies in depth sections tend to join in a single body.*

Introduction

In framework of FP7 project HP-SEE we have experimented the gravity anomaly inversion in parallel systems using OpenMP and MPI parallelization techniques (computational physics application GIM – Geophysical Modeling & Inversion, http://wiki.hp-see.eu/index.php/GIM).

The geophysical inversion [1] remains a difficult ill-posed problem [2], which requires for its solution the the extrapolation of data from a 2D surveyed surface anomaly to a 3D geosection representing the delineation of differentiated geological structures. Decades of work are dedicated to the inversion problem, with solutions obtained mostly for 2D geosections in certain conditions ([3], [4]). Recently the paralel processing is used in several cases as in [5], [6]. Due to the "ill-posed" problem, solutions remain "uncertain" [7]. An example of this uncertainty is presented in the inversion of a two cuboid bodies model in [8]: there is lack of contrast between inverted body and the surrounding rocks, and a ireal "syncline structure" joining the two bodies (Fig. 1).

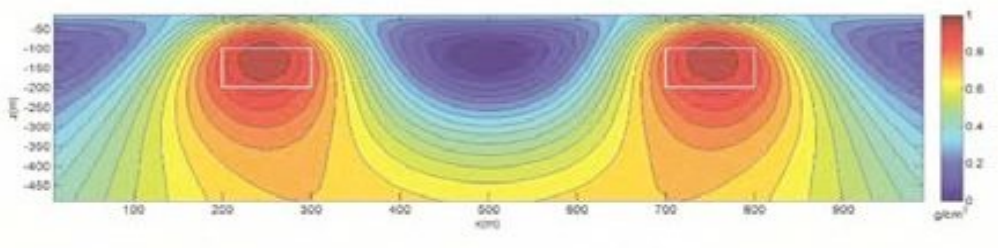

Fig. 1 – Two body model inversion from [6]

Our work had two directions: to analyze the scalability of the algorithm in parallel systems in time domain, and to evaluate the quality of approximation of inverted solutions. A detailed analysis of the scalability is presented in a number of publications [9],[10],[11],[12],[13]. In the actual paper we focused more on geophysical aspects of the problem.

Methodology

We selected the gravity as the simplest case of physical fields from calculation point of view [14]. The algorithm idea is obtained from the CLEAN algorithm [15]. We considered the 3D geosection as an array of cuboid elements represented by their central node where the mass of the cuboid is concentrated (Fig. 2).

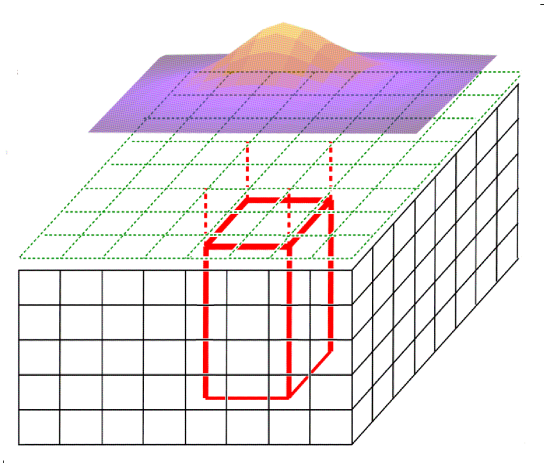

Fig. 2 – 3D geosection model

The algorithm works iteratively, starting from the initial homogeneous geosection with mass density zero. In each iteration the best 3D node is selected, which anomaly shape gives the best approximation of the residual anomaly; the mass density of this node is updated with a predefined quantity (mass density step) and the effect of the change is subtracted from the residual anomaly. A predefined maximal mass density was applied. Error calculation for the approximation of the surface anomaly was done using the weighted least squares error within a window into the respective 2D array of data.

The iterations continue until some termination criteria is fulfilled. Two termination criteria were experimented: the anomaly approximation error became less than a predefined threshold, or until the required change of the mass density for the best 3D node was less than half of mass density step. It resulted that there was no significant difference of results obtained with each of termination criteria.

The complexity of the algorithm was evaluated on the basis of the geometrical mean of the number N of 3D nodes in edges of 3D geosection. Number of iterations depended on the quantity of incremental steps of mass density necessary to fill a certain 3D volume, with an order of O(N^3) iterations. For each iteration the number of elementary calculations – the effect of one 3D geosection node in one 2D point of the anomaly – was O(N^5), resulting to an order of O(N^8) for the calculation time.

The case of multi-modal anomalies was considered and two different formulas were used for the least squares error to identify the best 3D geosection node:

- simple least squares formula
- weighted least squares formula, using as weight for each 2D point the relative value of the 3D node anomaly effect in that point

In both cases the error was calculated within a window with variable size based on the depth of each 3D node, in order to include in the error only 2D points where the 3D node anomaly was significant (Fig. 3).

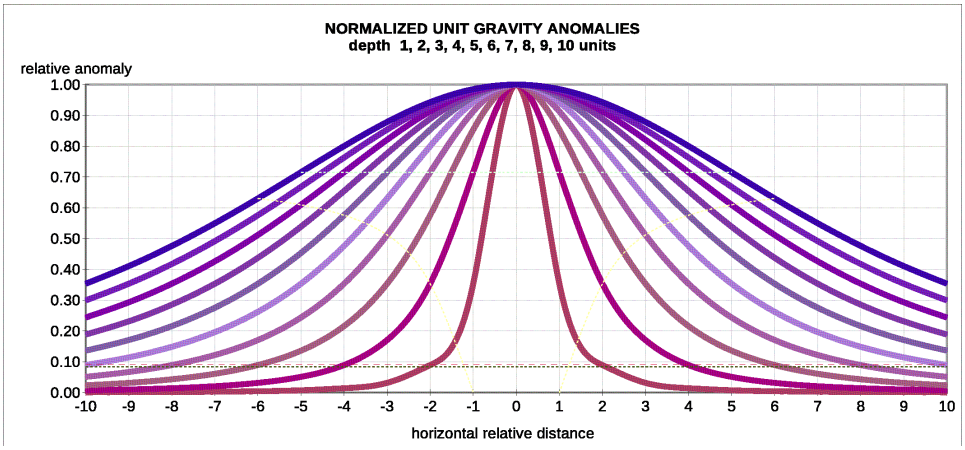

Fig. 3 – relative weights and window sizes depending on the shape of anomaly

Experiments with synthetic models were done with a geosection 4000m*4000m*2000m discretized with 11x11x6, 21x21x11 and 41x41x21 nodes. Respective 2D arrays were used for the surface anomaly. Bodies were represented by vertical prisms with section 400m*400m and different heights. Inversion for models with single body and two bodies was computed. Several two-body models were used, varying the height and the depth of bodies. In all models bodies with mass density varying in the range of 3 – 5 G/cm^3 were used.

For each model, based on the respective discretization schema, the direct calculation was used to obtain the anomaly, which was used for the inversion.

Two field cases were experimented, using maximal mass densities of 0.3 G/cm^3 and 5 G/cm^3. In the first field case the anomaly was centered within the 2D array, while in the second field case it was composed of one positive and one negative anomaly situated at the sides of the 2D array.

Computational Results of Models

Single body model was used to evaluate the runtime of the application. The anomalous body with mass density 5 G/cm^3 was designed 400m*400m*1800m in depth 200m. The anomaly and inverted body are presented in Fig. 4:

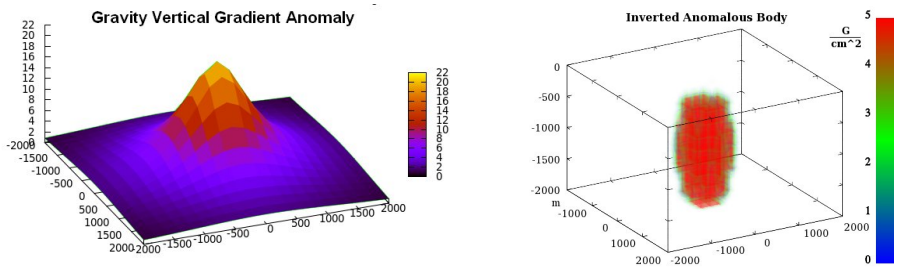

(a) *(b)*

Fig. 4 – The gravity anomaly of prismatic body (a); and inverted body (b)

The mean absolute error of the inverted anomaly was 0.0438 (1.54%) with a standard squared deviation 0.0195. The spatial distribution of the absolute error is given in Fig. 4.c:

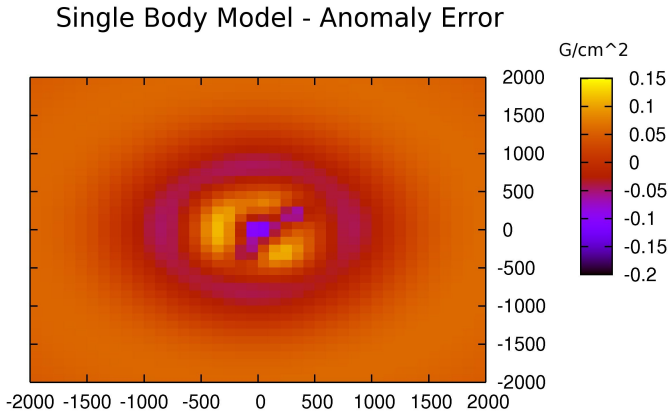

Fig. 4.c – Distribution of inverted anomaly absolute error

The contrast of mass density between the anomalous body and surroundings resulted satisfactory. Further tests showed that the algorithm has the tendency to reach maximal permitted mass density despite the density of original body (Fig. 5).

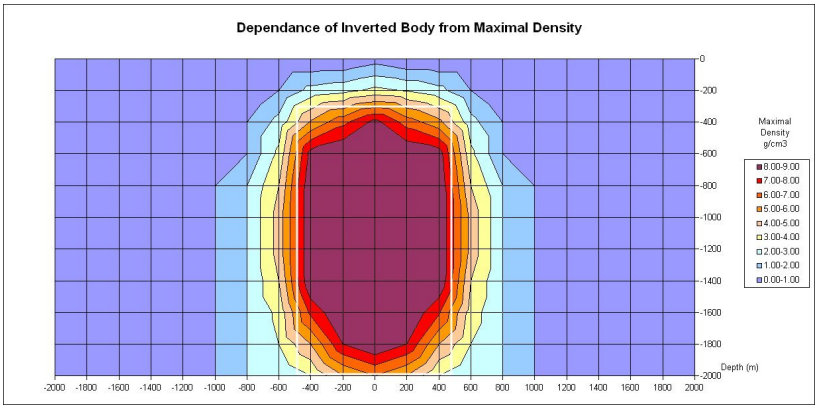

Fig. 5 – Variation of body delineation due to maximal permitted mass density

The number of iterations and the variation of mean absolute error of the approximation of anomaly due to the increase of number of discretization nodes is shown in Fig. 6:

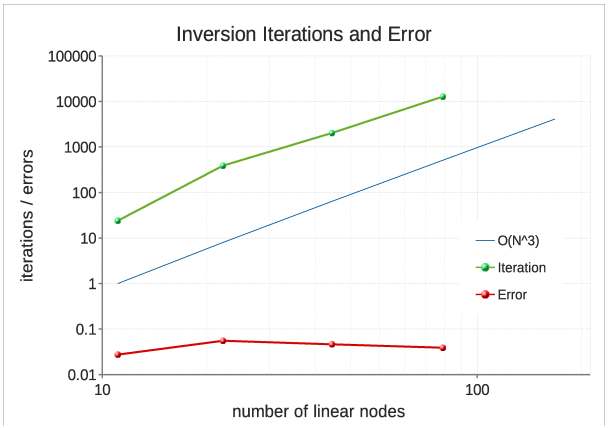

Fig. 6 – Iterations and Errors by model size

The error variation represents little dependence from the model size because of the fact that the anomaly was calculated and inverted for each model discretization, instead of using the

same anomaly for different model discretizations.

The runtime dependence from the model size and the number of computing cores is presented in Fig. 7. Both OpenMP and MPI gave similar results. The scalability of iterations follows the expected order of magnitude O(N^3).

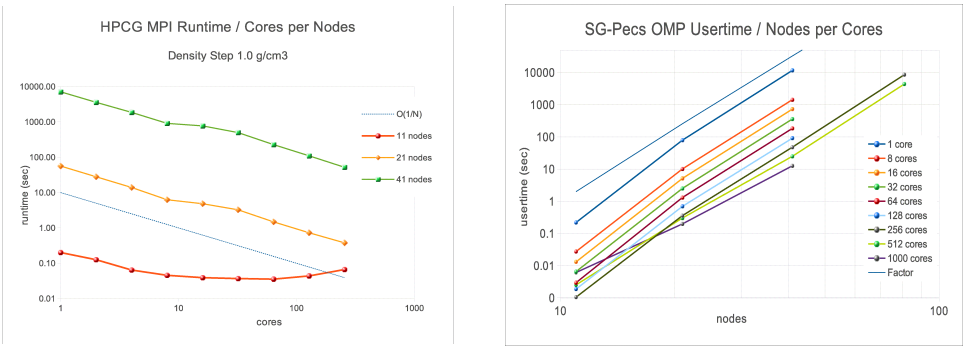

Fig. 7 – Runtime per computing cores and model size (factor=O(N^8))

For small models the runtime increases with multiple computing cores due to interprocess communication overheads. The same effect is the cause of the step observed when number of computing cores increases from 8 to 16 cores – the parallel system HPCG is composed of computer nodes with 8 cores interconnected through a switch, which offers less bandwidth compared with the BUS that interconnects cores within the same computer node.

The case of two bodies' models was done for prismatic bodies with different density mass. The first experiment was done with prisms of 400m*400m*1600m arising from the floor of the 3D geosection to the depth -400m, distanced 1200m from each other. The 3D geosection was discretized with 41x41x41 nodes. The shape of two-modal anomaly is given in Fig. 8a:

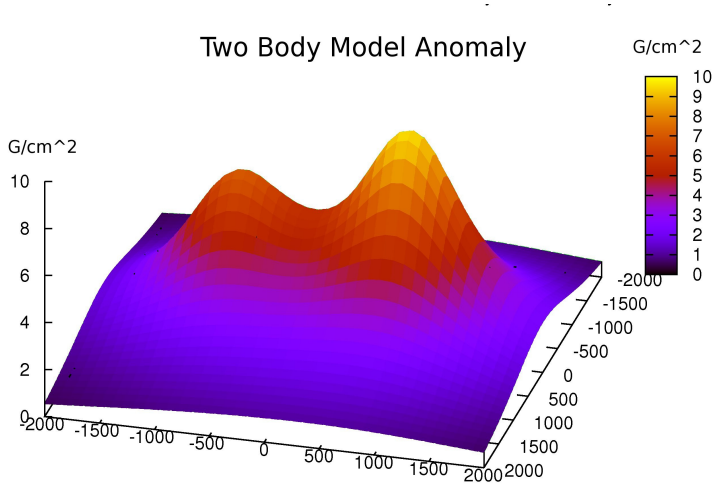

Fig. 8.a – Anomaly of two bodies' model

The tendency of algorithm is to approximate firstly the overall anomaly and afterwards to deal with local modes, which lead to the creation of an ireal "syncline" in depth between two bodies (Fig. 8.b, similar to the fig. 1 of [6]).

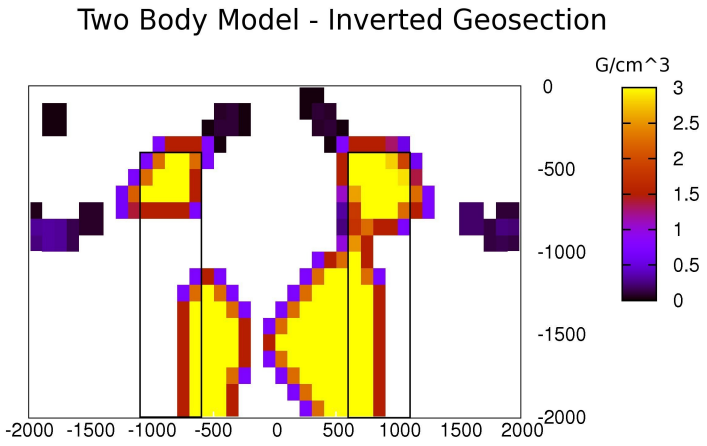

Fig. 8.b – Inverted central cross-section of the geosection (black empty rectangles are original bodies)

The mean absolute error resulted 0.0112 (0.41%) with a standard squared deviation 0.0054. The spatial distribution of the inverted anomaly absolute error if given in Fig. 8.c:

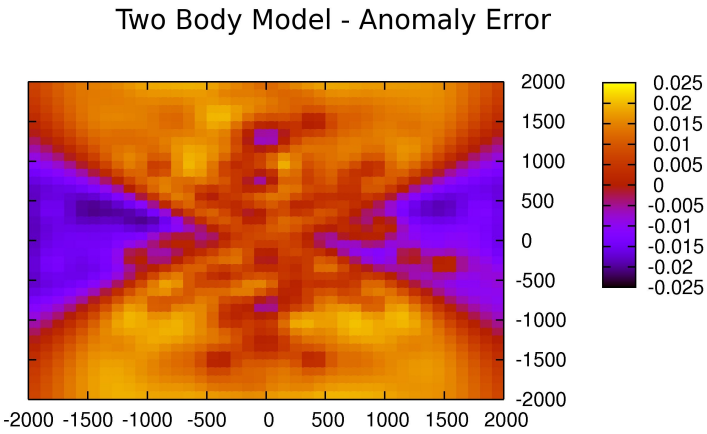

Fig. 8.c – Distribution of anomaly absolute error

The original anomaly shape is elongated through the line that joins both separated bodies, while in the inverted geosection most of the anomalous mass in depth is joined as in one body, which gives for the respective anomaly a more rounded shape and causes the "butterfly" distribution of the anomaly error.

The second experiment was done using two cuboid bodies of 400m*400m*600m situated in three different depths -400m, -800m and -1400m distanced 1200m from each other. The 3D geosection was discretized with 21x21x11 nodes with step 200m. The mass density of two cuboids was 2 G/cm^3 and 3G/cm^3, while the maximal permitted mass density for the inversion 5G/cm^3.

Respective anomalies are given in Fig. 9. For deep bodies the anomaly becomes uni-modal and that phenomenon makes difficult the separation of two anomalous bodies. The results fo the inversion are given in Fig. 10, with the position of original bodies delineated with empty black/white rectangles.

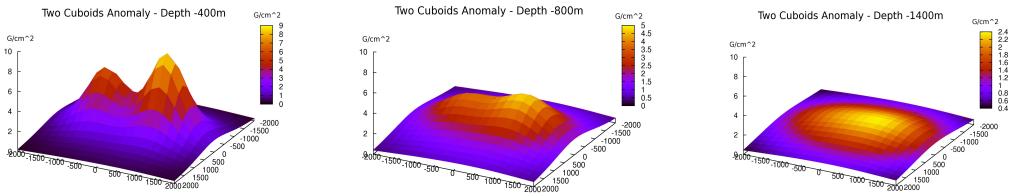

Fig. 9 – Anomalies of two cuboid model in dopths -400m, -800m, -1400m

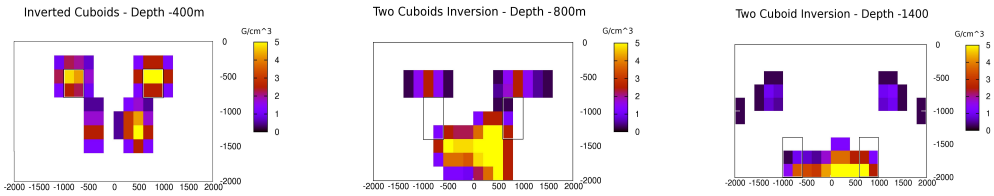

Fig. 10 – Two cuboids central cross-section of inverted 3D geosection

The mean absolute error of approximation of original anomalies with inverted ones resulted respectively 0.0637, 0.1153 and 0.0347 G/cm^2.

For the second case with two bodies in mid-depth their individual anomalies are not well separated, which reflects the cause of the greater error in this case. Going more in depth individual anomalies merge with each other and become more similar with a single body anomaly.

Inversion of Real Field Cases

The first field case was a section of gravity field composed by partial positive and negative anomalies (Fig. 11.a):

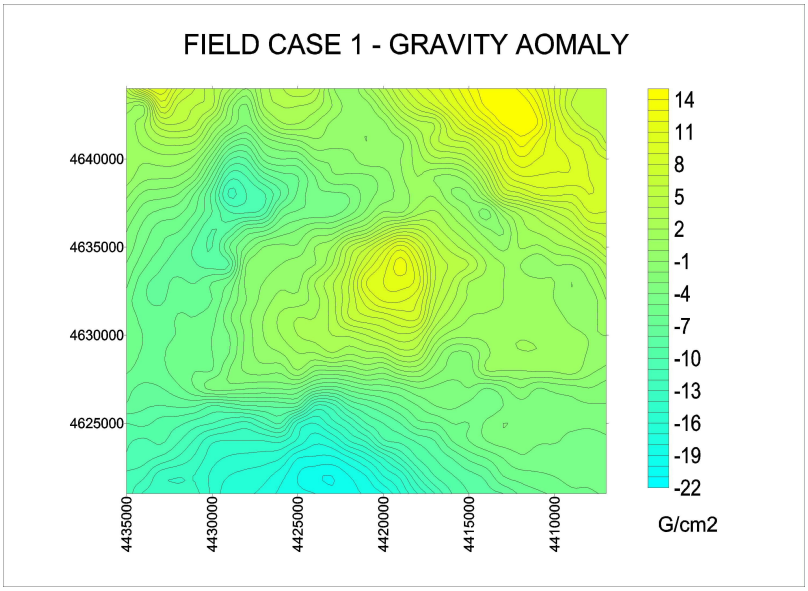

Fig. 11.a – Field case gravity anomaly

The inverted 3D gosection is presentetd in Fig. 11.b:

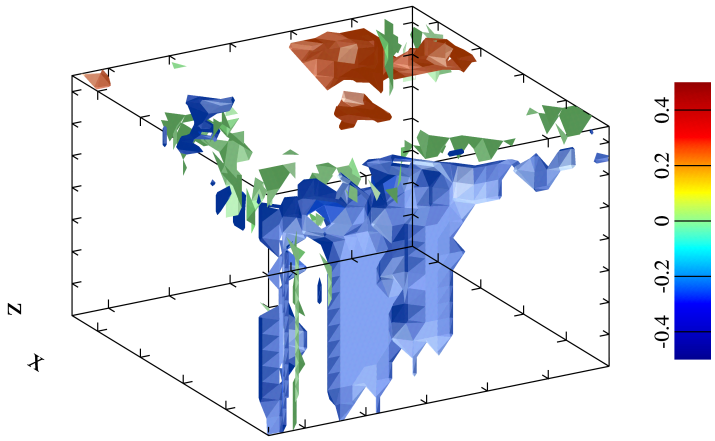

Fig. 11.b – Inverted 3D geosection (mass density in G/cm^3)

Calculation of the inversion was done using maximal permitted mass density of 0.3 G/cm^3.

Two distinct structures are identified in the inverted geosection: the first one is shallow with mass density greater than surrounding rocks (“positive” density, brown area in the figure), and the second one with mass density lower than surrounding rocks (“negative” density, blue area in the figure) and vertically extended.

For higher densities the body with “negative” density was constricted in the shape of a cylinder in mid-depth of the geosection (not presented in the figure).

The spatial distribution of the absolute error of the inverted anomaly is given in Fig. 11.c:

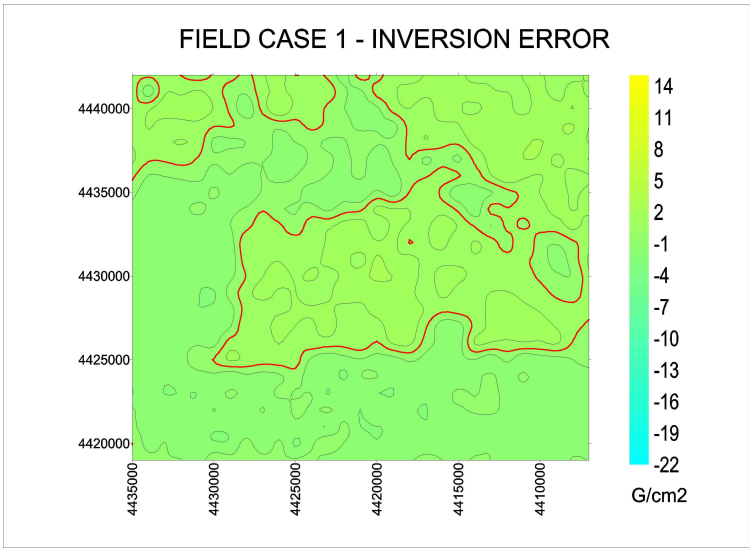

Fig. 11.c – Inverted anomaly error

The absolute error varied between (-2:+2) G/cm^2 for an inverted anomaly that varied between (-20:+14) G/cm^2

The second field case was a Bouguer Anomaly from an area with ophiolites (Fig. 12.a).

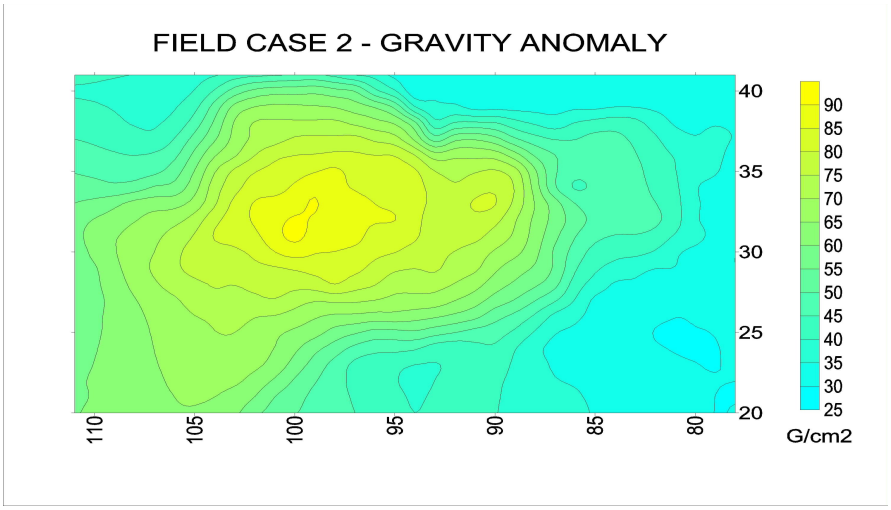

Fig. 12.a – Bouguer Anomaly over ophiolites

The inverted 3D geosection is given in Fig. 12.b, with the maximal permitted mass density was 0.3 G/cm^3, comparable with the expected contrast between categories of rocks in the area.

The anomalous body obtained by the inversion had the shape of an overturned bowl of higher density compared with surrounding rocks.

For greater maximal permitted densities the anomalous body resulted constricted as a cylinder in deepest central part of the geosection (not included in the figure).

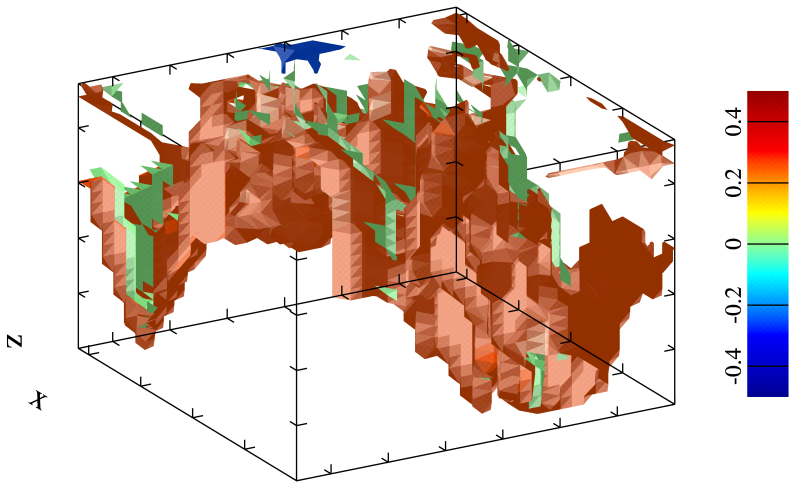

Fig. 12.b – Inverted 3D geosection, mass density in G/cm^3

The absolute error resulted in the range of (-3:+3) G/cm^2, for an inverted anomaly that varied between (+25:+100) G/cm^2 (Fig. 12.c).

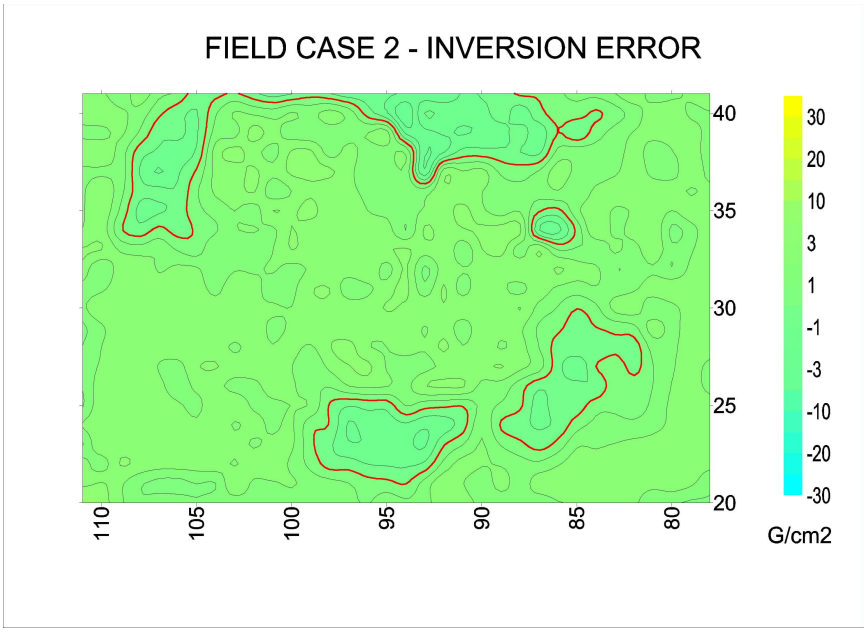

Fig. 12.c – Anomaly error (red isolines represent zero values)

In both cases the increase of the mean error was observed when the maximal permitted mass density was increased.

Conclusions

The algorithm works with starting conditions of mass density zero for the whole 3D geosection. The solution is approached step by step improving the mass density of one single 3D node (representative of one cuboid element) with a predefined mass density "quant". Mathematically it is searching of a global optimum through local improvements leading to a local optimum.

The scalability of the algorithm run in high performance parallel computing systems matched the expectations with an order of magnitude O(N^8), where N is geometrical mean of the linear size in number of discretization nodes of the 3D geosection. With a reasonable runtime of several hours using several hundreds of parallel computing cores only models with modest resolution (number of 3D nodes) were possible making the algorithm applicable for gravity studies; for other physical fields that are associated with thin geological structures and require high resolution the application of the algorithm would be difficult considering the runtime.

The algorithm gave good results for single body structures – the case when global and local optimums are the same. For multi-body structures (multi-modal anomalies) the results are disputable, the tendency is to fail in separation of bodies in depth giving false syncline structures. Nevertheless good separation of bodies was obtained for a two modal positive – negative field case anomaly. The conclusion is that interpretation of inversion results for multi-modal anomalies requires careful correlation with other geological data.

The algorithm works in parallel and cluster (grid) platforms using MPI. It may be easily modified to work for regional variations of magnetic anomalies as well. A new work direction for the the future is combination of the algorithm with other optimum searching methods and implementation in Graphical Processing Units (GPU) both in desktop and parallel platforms.

Acknowledgments: This work makes use of results produced by the High-Performance Computing Infrastructure for South East Europe's Research Communities (HP-SEE), a project co-funded by the European Commission (under contract number 261499) through the Seventh Framework Programme. HP-SEE involves and addresses specific needs of a number of new multi-disciplinary international scientific communities (computational physics, computational chemistry, life sciences, etc.) and thus stimulates the use and expansion of the emerging new regional HPC infrastructure and its services. The work is supported by the HP Cluster Platform Express 7000 operated by the Institute of Information and Communication Technologies, Bulgarian Academy of Sciences in Sofia, Bulgaria and the SGE system of the NIIFI Supercomputing Center at University of Pécs, Hungary. Full information is available at http://www.hp-see.eu/.

References

1. Sen M., Stoffa P. Global Optimization Methods in Geophysical Inversion. Elsevier Science B.V. (1995)
2. Hadamard, J. Sur les prolemes aux derivees partielles et leur signification physique: Bull Princeton Univ., 13, l-20 (1902)
3. Shamsipour P., Chouteau M., Marcotte D., Keating P. 2010. 3D stochastic inversion of borehole and surface gravity data using Geostatistics. EGM 2010 International Workshop, Adding new value to Electromagnetic, Gravity and Magnetic Methods for Exploration Capri, Italy, April 11-14, 2010
4. Silva J., Medeiros W.E., Barbosa V.C.F. Gravity inversion using convexity constraint. Geophysics; January-February 2000; v. 65; no. 1; p. 102-112 (2000)
5. Loke M.H. and Wilkinson P. Rapid Parallel Computation of Optimized Arrays for Electrical Imaging Surveys. Near Surface 2009 – 15th European Meeting of Environmental and Engineering Geophysics Dublin, Ireland, 7 - 9 September 2009
6. Wilson G., Čuma M., and Zhdanov M. S. Massively parallel 3D inversion of gravity and gravity gradiometry data. PREVIEW - The Magazine of the Australian Society of Exploration Geophysicists, June 2011
7. Wellmann F.J., Horowitz F.G., Schill E., Regenauer-Lieb K. Towards incorporating uncertainty of structural data in 3D geological inversion. Elsevier Tectonophysics TECTO-124902. http://www.elsevier.com/locate/tecto (2010). Accessed 07 Sept 2010
8. Zhdanov M. S., Wilson G. A., Xiaojun Liu. 3D imaging of subsurface structures using migration and regularized focusing inversion of gravity and gravity gradiometry data. In R. J. L. Lane (editor), Airborne Gravity 2010 - Abstracts from the ASEG-PESA Airborne Gravity 2010 Workshop, published jointly by Geoscience Australia and the Geological Survey of New South Wales, Geoscience Australia Record 2010/23.
9. Frasheri N., Cico B. Analysis of the Convergence of Iterative Gravity Inversion in Parallel Systems. Submitted in ICT Innovations 2011 Conference, Macedonian Academy of Sciences and Arts (MANU), Skopje, 14-16 September 2011. Springer Advances in Intelligent and Soft Computing 150: ICT Innovations 2011 (ed. L. Kocarev). Springer-Verlag 2012
10. N. Frasheri, S. Bushati. An Algorithm for Gravity Anomaly Inversion in HPC. SYNASC 2011 - 13th International Symposium on Symbolic and Numeric Algorithms for Scientific Computing, September 26-29, 2011, Timisoara, Romania. SCPE: Scalable Computing: Practice and Experience vol. 13 no. 2, pp. 51-60

(http://www.scpe.org/index.php/scpe).

11. Frasheri N. and Cico B. Convergence of Gravity Inversion using OpenMP. Information Technologies IT'12, Zabljak Montenegro, Feb 27 – March 02, 2012.
12. N. Frasheri, B. Cico. Reflections on parallelization of Gravity Inversion. HP-SEE User Forum, 17-19 October 2012, Belgrade, Serbia.
13. N. Frasheri, B. Cico. Scalability of geophysical Inversion with OpenMP and MPI in Parallel Processing. ICT Innovations 2012. 12 – 15 September, Ohrid, Macedonia. Springer Advances in Intelligent Systems and Computing 207, Smile Markovski and Marjan Gusev (Eds.) ICT Innovations 2012 Secure and Intelligent Systems, 2013.
14. Lowrie W. Fundamentals of Geophysics. Cambridge University Press (2007)
15. Högbom, J.A. Aperture Synthesis with a Non-Regular Distribution of Interferometer Baselines. Astr. Astrophys. Suppl., 15, 417 (1974)